Influences of major flood sediment inputs on sedimentary and geochemical signals archived in a reservoir core (Upper Loire Basin, France)

E. Dhivert [a], C. Grosbois [a,*], A. Coynel [b], I. Lefèvre [c], M. Desmet [a]

[a] Université François Rabelais de Tours, EA 6293 GéHCO, Parc de Grandmont, 37200 Tours, France
[b] Université de Bordeaux, UMR 5805 CNRS EPOC, Av. des universités, 33405 Talence cedex, France
[c] Laboratoire des Sciences du Climat et de l'Environnement, UMR CNRS/CEA/UVSQ 1572-IPSL, 91198 Gif-sur-Yvette, France

ABSTRACT

The Villerest flood-control reservoir was built in the Upper Loire River (France) during the early 1980s, downstream from the most important industrial and coal-mining area of the basin. This reservoir has constituted an important trap for sediments and associated pollutants since its operation in 1984. A 154-cm-long core was recovered in 2010 in the deepest area of the reservoir and shows the influence of sedimentary infill processes on aggradation rates and selected chemical patterns. During dam operations, the lacustrine aggradation rate is not linear because of three turbiditic-like layers resulting from sediment-laden underflows during major flood events in 1996, 2003 and 2008. These three events contribute to 43% of the 151 kg·m^{-2} of accumulated sediments over the 1984–2010 period. Trace element solid sources are activated during these floods as selected metals present the highest enrichment factors, levels never reached during interflood periods. In addition, sedimentological and detrital geochemical signals during these events influence anthropogenic trace element signals by a variable dilution effect (maximum during the increasing discharge stage). Hence, coupling sedimentological and geochemical approaches allows us to understand the sedimentary infill dynamics and, more specifically, to take into account the influence of floods on the temporal trajectories of pollutants.

© 2014 Elsevier B.V. All rights reserved.

1. Introduction

At the basin scale, the spatial distributions of the sedimentary contamination of metallic pollutants are largely controlled by the settling capacity of fine-grained sediments (<63 μm; Horowitz and Elrick, 1987; Walling et al., 2003). Over the last 50 years, dam constructions highly modified the transfer of sediments in hydrosystems by constituting storage areas for transported sediments (Vörösmarty et al., 2003). The coarsest sediments are mostly deposited in the delta part of the reservoirs, while the finest sediments settle in the deepest area (Fan and Morris, 1992; Morris et al., 2008; Ziegler and Nisbet, 1995). Potentially polluted sediments trapped in reservoirs can then become a source of contamination for biota, interstitial and surface waters by pollutant diffusion at the water–sediment interface, by organic matter mineralization, or by reworking within pollutant-bearing phases during dam exploitation (maintenance, dredging and/or emptying, dam flushing) (Audry et al., 2010; Coynel et al., 2007). However, these reservoirs also offer good opportunities – as do lakes – to find preserved contamination records (Audry et al., 2004; Castelle et al., 2007), particularly

in fluvial systems where the high spatial and temporal variability of aggradation rates managed floodplain edifications (Bábek et al., 2008; Desmet et al., 2012; Mourier et al., 2014; Walling and He, 1997; Walling and He, 1998; Walling et al., 1997). This is particularly important for rivers affected by artificial width contraction (Arnaud-Fassetta, 2003). Numerous studies address the annual and seasonal sediment trapping yield of large dam reservoirs (e.g., Dai et al., 2008; Yang et al., 2002) and associated-sediment pollutant dynamics over time, especially during high discharge events (Vukovic et al., 2014; Ye et al., 2011), but sedimentary infill processes and their influence on aggradation rates and sediment chemical temporal patterns are poorly understood. Thus, the origins of the trapped sediment and settling conditions constitute a key point towards building the temporal trends of pollutants, anthropogenic sources and their variations at a basin scale.

The Villerest flood-control reservoir, built in the Upper Loire River (France) downstream from an important industrial and coal-mining area (Saint Etienne; Fig. 1), largely contributes to the retention of potentially polluted sediments, complementing the other large dam in the basin (Grangent Dam, Fig. 1). The present study uses sedimentological and geochemical approaches to characterize the sediment dynamics and associated TE during infilling processes in a high-order stream reservoir and shows the main influence of high discharge events on TE temporal trends.

---

* Corresponding author. Tel.: +33 247367002.
 E-mail address: cecile.grosbois@univ-tours.fr (C. Grosbois).

2. Study area and methodology

2.1. Main geographical and geological characteristics of the study area

The Loire River basin (117,800 km^2) is among the ten largest W-European basins and the largest in France. The Upper Loire (Strahler stream order of 6), upstream from the studied station at the Villerest Dam, is 260 km long and drains a basin of 6516 km^2. According to the French geological survey (infoterre.brgm.fr, 2013), it contains four main geological units (Fig. 1): (i) Variscan plutonic rocks (granites, gneiss and micaschists, aged between 500 and 300 Ma) covering 63% of the basin area; (ii) volcanism between 20 Ma and 300 ka, representing approximately 15% of the basin area and only located in the S-E part; (iii) sedimentary bedrock of Carboniferous (mainly sandstones) and Oligocene–Miocene age (fluviolacustrine deposits such as sands, marls and clays), corresponding to 4 and 12%, respectively, of the upper basin surface; and (iv) Quaternary alluvia along the river covering 5% of the surface.

According to the Villerest Dam managers (EPL, www.eptb-loire.fr, 2013), the hydraulic structure was built between the late 1970s and 1983, and water filling operations occurred by steps between 1983 and 1984. The dam has been in operation since 1984 with a mean water reservoir of 128 Mm^3, approximately 36 km long (influencing 14% of the upstream main channel length) and no wider than 900 m with a maximum depth of 60 m. The water level varies by 11 m over a year as the current exploitation of the reservoir allows two operating modes in relation to the hydrological cycle: i) during the spring and autumn, the water level is at the minimum to control winter flood outflows; ii) conversely, at the beginning of summertime, the water level is at the maximum to guarantee a minimal low flow (at least 12 m$^3 \cdot$s^{-1} at the Villerest gauging station, 1 km downstream from the dam). The Villerest Dam is also a hydroelectric power plant that remains in operation all year.

The hydrological regime in the upper basin is a balance of oceanic and Mediterranean influences with additional snow-melt in the spring (Dacharry, 1974). The resulting annual hydrological cycle at the Feurs gauging station, 19 km upstream of the dam's influence, is characterized by winter high flows with floods in the autumn, winter and/or spring. During the high flow for the 1984–2010 period, the highest monthly discharge was 64.3 m$^3 \cdot$s and the summer low flows show a minimum of 10.5 m$^3 \cdot$s (www.hydro.eaufrance.fr, 2013). Since the beginning of the dam's construction, several major flood events occurred (Fig. 1b): (i) 3 major floods with a greater than 50-year flood average daily discharge calculated over the period (1400 m$^3 \cdot$s^{-1}) in November 1976 (1410 m$^3 \cdot$s^{-1}), December 2003 (1570 m$^3 \cdot$s^{-1}) and November 2008 (1490 m$^3 \cdot$s^{-1}); (ii) a greater than 20-year flood average daily discharge (1200 m$^3 \cdot$s^{-1}) in May 1983 (1340 m$^3 \cdot$s^{-1}), just before water filling operations started in the Villerest Dam; (iii) additional important floods occurred in May 1977 (1050 m$^3 \cdot$s^{-1}) and September 1980 (1060 m$^3 \cdot$s^{-1}). All of these major floods resulted from heavy rainfall episodes in the upstream basin. They usually took place throughout the basin with maximum discharges at the same time in the Loire main stream and its major tributaries.

2.2. Analytical methods

The coring site (45°58′54″N, 4°2′15″E) is located 200 m upstream from the Villerest Dam in the deepest zone of the reservoir (57 m deep at the coring site) when the water level in the reservoir was the lowest. The core was recovered from a platform ship in September 2010 with a UWITEC gravity corer fitted with a 2-m long and 90-mm diameter plastic liner. At the laboratory, only sediments from the middle of the liner were sampled in 2 cm-slices with a ceramic knife. The slices were then stored in acid-washed plastic containers to prevent metallic contamination. Neither gas bubbles nor living organisms and/or bioturbation features were clearly observed when slicing. The dry bulk density
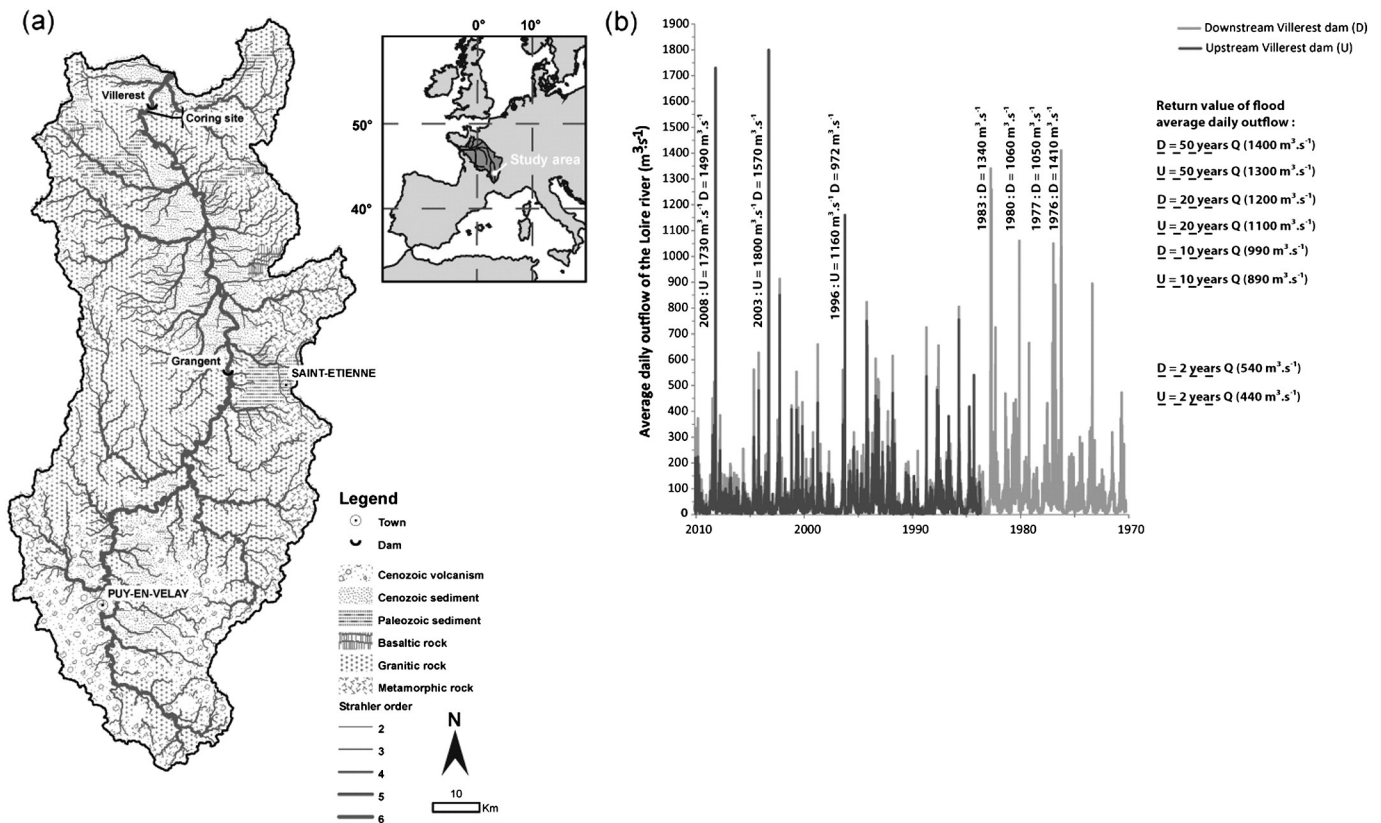

Fig. 1. a — Localization of the studied area, the coring site in the Villerest reservoir, the geology and the 2 main towns (Saint Etienne >500,000 inhabitants; Le Puy en Velay >60,000 inhabitants); b — Daily discharge variations upstream and downstream of the studied dam site since 1970 (data from www.hydro.eaufrance.fr).

$(kg \cdot m^{-3})$ was determined as the weight of dry material divided by the volume of the container, and the water content (%) was calculated from the weight difference between the fresh and dry sediments. Particle size analyses were performed after a 1-min ultrasonic step with a Malvern Mastersizer 2000 laser diffraction microgranulometer on each fresh 2-cm core slice (measurement range between 0.02 and 2000 µm). Although leaf and brushwood remains were present in low amounts in the studied core, they disturbed the measured grain-size signal, so macroscopic organic remains were manually removed before the measurements. The grain-size median (D_{50}), the ten percentile (D_{10}), the ninety percentile (D_{90}) and the cumulative volumetric percentage of clay (<2 µm), silt (2–63 µm) and sand (>63 µm) were computed with a Gradistat spreadsheet (Blott and Pye, 2001) using the Folk and Ward geometric method (Folk and Ward, 1957).

The radiometric analyses were performed on approximately 50 g of <2 mm core material in air-tight plastic boxes for a 24 h gamma-counting. Very low-background detectors, namely, coaxial HP Ge N-types, were used for gamma spectrometry (8000 channels, low back-ground). The efficiencies and backgrounds were periodically controlled with internal soil and sediment standards, pure KCl samples, and IAEA standards (Soil 6, 135 and 375). ^{137}Cs was detected with an energy peak at 661 keV in a spectrum area free of any interference. The activities were corrected to the time of the collection period, and the uncertainty of the measurements was approximately 0.5% with a detection limit of 0.3 Bq·kg. The ^{137}Cs artificial radionuclide activity is commonly used in bed sediments as a time calibration, using 3 events in Western Europe: (i) its introduction in 1950 in the atmosphere by the first important nuclear weapon tests (NWT), (ii) the maximum ^{137}Cs atmospheric fallout in 1964 (atmospheric ^{137}Cs emissions decreased after 1964 thanks to the October 1963 nuclear test ban treaty, Walling and Bradley, 1990; Klaminder et al., 2012) and (iii) the 1986 fallout peak following the Chernobyl nuclear power plant disaster (C-NPPD). We also used the top of the core between 2 and 0 cm, which corresponds to the sampling period (2010 here).

Part of each air-dried material slice was sieved through <63 µm disposable Nylon mesh. The chemical composition was also determined with the <63 µm fraction to limit the grain-size and associated mineralogical influence. The selection of fine-grained sediments for the geochemical analyses is particularly important in the Loire River context, where the sandy fraction is very heterometric and the mineralogical composition of the sediments depends on the grain-size of the particles (Macaire et al., 2013; Valverde et al., 2013). Representative 0.5 g of dry <63 µm material was digested in a Teflon beaker in a tunnel oven with $LiBO_2–Li_2B_4O_7$. After the samples were dried, the residues were completely re-dissolved with HNO_3 acid. Additional splits of 0.2 g were digested by hot Aqua Regia (95 °C) for the determination of trace element (TE) abundances. The total contents of the major and minor elements were analyzed by ICP-AES (Jobin-Yvon 70; Govindaraju and Mervelle, 1987), and the trace elements were analyzed by ICP-MS (Perkin Elmer 5000, Govindaraju et al., 1994), except for Hg, which was analyzed by cold vapor AAS (Perkin Elmer 5100). The total carbon (TC) and total sulfur (TS) were analyzed by O_2 flow combustion at 1000 °C using a LECO SC 144 DR. All of the digestion processes and analyses were quality-checked by the analyses of one sample out of every ten and internal reference materials. The accuracy was within 5% of the certified values and the analytical errors better than 10% rsd for the TE concentrations (Table 1).

3. Results and discussion

3.1. Characterization of depositional conditions

3.1.1. Sedimentary description of the Villerest core

The sedimentological analysis of the 154 cm long core consists of a visual and textural description (Fig. 2) in addition to a comparison of the grain-size distribution in the sedimentary layers with the C–M

diagram (Passega, 1957, 1964; Fig. 3). This diagram allows the characterization of the particle depositional conditions according to the ninety-nine percentile (D_{99}) and the median grain-size (D_{50}) distribution, called the C and M parameters, respectively. In this approach, the higher the C and M values are and the more the grain-size distribution is parallel to the C–M line, the more energetic the depositional environment is. The grain-size distribution of these studied sediments, measured with a laser granulometer, should be considered with caution because of their fine-grained and very poorly sorted texture (Pye and Blott, 2004). Because the grain-size measurement reproducibility was low for D_{99}, D_{90} was used as the C parameter to be more representative. Throughout the entire core, three sedimentary units have been identified:

- The deepest unit 3 (128–154 cm), is also the coarsest unit. It is composed of very coarse silts to fine sands ($59 < D_{50} < 284$ µm) (Fig. 2). The percentage of sand ranges from 48% (126–128 cm) to 88% (136–138 cm) with the highest D_{90} of the entire core (312–632 µm). According to the Valverde et al.'s (2013) study, which defines the characteristics of stream sediments in the Upper Loire sub-basin ($D_{50} > 1000$ µm and $D_{90} > 1100$ µm), and Bravard et al.'s (2013) interpretations of the CM image, the grain-size distribution of this sedimentary layer looks like a river bank deposit in a proximal position from the river channel (low variability of D_{90} compared to D_{50}, characteristic of the RS segment; Fig. 3). Hence, unit 3 can represent the fluviatile domain, i.e., sediments deposited in energetic conditions, but they may also have been reworked during the dam construction.

- On the other side, the upper unit 1, from 84 cm up to the surface, corresponds to the finest very poorly sorted particles, mainly silts with clays (73–87% silts, Table 1). The D_{50} ranges from 7.3 µm (64–66 cm deep) to 19.8 µm (42–44 cm). Immediately after the core opening, laminated sedimentary layers were visually identified at the 54–84 cm ($7 < D_{50} < 14$ µm); 50–58 cm ($8 < D_{50} < 12$ µm); 19–30 cm ($10 < D_{50} < 14$ µm), except within 22–24 cm; and 0–6 cm depths ($9 < D_{50} < 10$ µm; Fig. 2), showing centimeter alternations of lighter and darker bands. In these sedimentary layers, the alternation of sediment colors is not associated with textural variations. The grain-size distribution of these sequences is not parallel to the C–M line (Fig. 3). Therefore, they consist of fine-grained sediments that settled in a lentic environment since the dam began operation in 1984. Organic matter was not characterized, but darker layers should correspond to death biomass depositions after summertime. In addition, well-defined coarser and lighter layers at the 58–64 cm, 30–50 cm and 6–19 cm depths (Fig. 2) do not fit in the predefined domain. All of these stacked intervals also present a larger grain-size distribution than the respective unit with a higher sand percentage. They all note various depositional processes. The 6–19 cm level presents vertical grain-size sorting (18.5% down to 8.6% sand with upward coarsening at the beginning until 14 cm deep), whereas the two other coarse levels show a hysteresis in the C–M diagram from fine to coarse grains and back to fine particles (10.0% up to 19.7% of sands with maximum grain size at 60–62 cm and 40–42 cm deep) (Fig. 3).

- Units 1 and 3 limit sharp grain-size transitions at 84 cm and 128 cm deep, which correspond to unit 2's boundaries. The color and textural composition of this sedimentary layer are homogenous. The percentage of silt clearly decreases downcore (from 78% down to 50%; Table 1), although the percentage of sand and D_{50} increases at the same time (up to 48% and to 56 µm, respectively; Fig. 2; Table 1). The grain-size distribution of this sedimentary unit draws a middle domain between the lacustrine and the fluviatile domains, which are not described in literature (Fig. 3). This can occur during dam water filling when the water level increases progressively. At the bottom of unit 2 (104–128 cm), the archived sediments are clearer and the grain-size distribution of this sedimentary layer presents similarities with the coarsest and lightest sequences of unit 1. Indeed,

Table 1

Selected major and trace element concentrations in the <63 μm sediments according to depth in the Villerest core; Cs activity; median grain-size (D_{50}) and percentages of grain-size fractions in the bulk sediment layers; preindustrial sedimentary concentrations used to calculate the enrichment factors (Grosbois et al., 2012). 1a — major elements; 1b — conservative trace elements, which present enrichment factors close to 1; 1c — trace elements with an anthropogenic influence (enrichment factors > 2); n.d. = not determined; <d.l. = under the detection limit.

Depth (cm)		^{137}Cs (2 s)	Median grain size	Sand percentage	Silt percentage	Clay percentage	Si	Al	Ca	Fe	K	Mg	Mn	Na	P	Ti
		(Bq·kg^{-1})	(μm)	(%)	(%)	(%)	%	%	%	%	%	%	%	%	%	%
0–2		10 ± 0.9	10.0	7.3	84.8	7.9	16.72	8.44	0.64	4.91	2.27	1.04	0.09	0.48	0.28	0.50
2–4			9.5	5.0	86.9	8.1	16.74	9.42	0.89	5.05	2.59	1.24	0.09	0.68	0.21	0.65
4–6			11.0	5.9	87.0	7.1	16.90	9.31	0.89	4.83	2.61	1.21	0.09	0.75	0.21	0.65
6–8	2008 flood event		12.7	8.6	85.4	5.9	16.57	9.42	1.11	5.07	2.66	1.30	0.08	0.76	0.20	0.74
8–10			15.8	11.5	83.7	4.8	16.87	9.17	1.00	4.91	2.56	1.22	0.09	0.76	0.20	0.72
10–12		15 ± 0.8	18.6	15.2	80.4	4.3	16.87	8.81	0.91	4.58	2.50	1.16	0.09	0.79	0.21	0.66
12–14			20.9	17.5	78.6	3.9	17.42	8.51	0.79	4.15	2.51	1.05	0.09	0.88	0.23	0.58
14–16			18.4	16.6	78.8	4.6	17.27	8.22	0.75	4.00	2.42	0.99	0.09	0.88	0.23	0.54
16–19			15.5	18.5	75.4	6.0	17.60	8.72	0.72	4.29	2.45	1.04	0.10	0.81	0.25	0.55
19–20			14.3	15.5	79.0	5.5	n.d.	n.d.	n.d.	n.d.	n.d.	n.d.	n.d.	n.d.	n.d.	n.d.
20–22		14 ± 1.6	16.9	22.6	72.7	4.7	16.10	8.81	0.69	4.89	2.24	1.06	0.12	0.50	0.35	0.50
22–24			13.4	17.7	76.6	5.7	17.10	8.33	0.69	4.82	2.26	1.04	0.11	0.56	0.36	0.50
24–26		12 ± 0.9	10.1	5.9	86.5	7.6	17.36	9.21	0.70	4.97	2.51	1.15	0.10	0.59	0.27	0.56
26–28			11.0	9.5	83.4	7.1	17.30	9.62	0.76	4.80	2.70	1.24	0.09	0.66	0.19	0.61
28–30			9.7	4.2	87.4	8.5	17.27	9.69	0.97	5.02	2.79	1.38	0.09	0.70	0.20	0.67
30–32	2003 flood event	12 ± 1.0	14.7	13.0	81.7	5.3	17.22	9.59	1.06	4.86	2.86	1.40	0.08	0.74	0.17	0.68
32–34			14.9	11.7	82.7	5.6	17.87	9.61	1.04	5.07	2.80	1.37	0.09	0.82	0.21	0.71
34–36		16 ± 1.0	15.8	12.0	82.9	5.1	17.85	9.33	0.99	4.82	2.79	1.31	0.09	0.86	0.21	0.68
36–38			16.7	13.4	81.6	5.0	17.54	8.89	0.91	4.48	2.66	1.19	0.09	0.85	0.22	0.62
38–40			19.9	17.6	78.4	4.1	18.66	8.85	0.86	4.38	2.68	1.13	0.11	0.91	0.28	0.59
40–42		15 ± 1.0	21.2	19.7	76.3	4.0	18.39	8.28	0.81	3.96	2.56	1.02	0.10	0.93	0.26	0.55
42–44			19.8	17.9	77.7	4.4	20.61	8.42	0.85	3.61	2.87	0.96	0.09	1.16	0.24	0.56
44–46			18.5	14.3	81.6	4.1	18.66	8.69	0.83	4.20	2.58	1.06	0.11	0.91	0.29	0.58
46–48			12.2	10.0	83.6	6.3	17.79	8.70	0.76	4.30	2.52	1.09	0.09	0.75	0.25	0.59
48–50			12.4	12.9	81.0	6.1	17.29	8.67	0.66	4.43	2.43	1.07	0.10	0.59	0.28	0.53
50–52		13 ± 0.9	9.0	14.5	75.1	10.4	17.01	7.86	0.61	4.63	2.06	0.95	0.12	0.42	0.41	0.46
52–54			10.0	11.6	80.4	8.0	16.47	9.52	0.62	4.86	2.50	1.14	0.10	0.49	0.30	0.52
54–56			12.3	14.9	79.3	5.8	16.99	9.14	0.69	4.85	2.57	1.12	0.10	0.53	0.32	0.54
56–58			7.8	6.8	82.9	10.3	16.71	8.90	0.74	4.98	2.44	1.10	0.12	0.54	0.38	0.56
58–60	1996 flood event		17.0	12.7	82.9	4.4	17.11	9.66	0.89	4.82	2.74	1.28	0.09	0.67	0.22	0.64
60–62		22 ± 0.9	18.4	14.5	81.4	4.1	17.16	8.80	0.85	4.57	2.58	1.20	0.11	0.71	0.26	0.58
62–64			14.0	12.3	82.7	5.0	17.31	8.65	0.77	4.50	2.46	1.12	0.12	0.70	0.28	0.56
64–66			7.3	9.6	79.9	10.5	16.62	8.74	0.67	5.03	2.37	1.06	0.15	0.47	0.41	0.52
66–68			12.1	12.1	81.6	6.3	17.14	9.05	0.70	4.83	2.45	1.12	0.14	0.50	0.34	0.55
68–70			10.6	11.1	81.9	7.0	17.72	9.34	0.76	4.57	2.67	1.22	0.10	0.59	0.24	0.56
70–72		21 ± 0.7	10.7	12.3	80.5	7.2	17.14	9.26	0.59	4.71	2.49	1.12	0.11	0.54	0.30	0.53
72–74			8.7	8.4	83.1	8.5	17.36	8.84	0.61	4.81	2.45	1.07	0.12	0.53	0.33	0.52
74–76		28 ± 1.3	9.5	13.5	78.1	8.5	17.05	8.99	0.58	4.82	2.47	1.06	0.12	0.52	0.37	0.52
76–78		43 ± 1.4	12.6	15.4	78.3	6.2	17.29	9.22	0.64	4.72	2.56	1.10	0.14	0.62	0.35	0.55
78–80		61 ± 1.9	9.9	12.1	79.6	8.3	17.26	9.36	0.64	4.82	2.56	1.14	0.12	0.58	0.33	0.54
80–82		124 ± 1.4	14.4	12.7	81.5	5.8	18.04	9.52	0.79	5.04	2.80	1.29	0.12	0.65	0.33	0.56
82–84		20 ± 1.2	18.0	21.0	74.7	4.3	17.93	8.35	0.88	4.55	2.64	1.12	0.14	0.74	0.36	0.52
84–86	Sediments deposited	9 ± 0.8	44.1	40.2	56.0	3.8	19.69	8.11	0.91	3.88	2.85	1.05	0.07	1.05	0.17	0.52
86–88	before or during the		39.9	36.9	58.8	4.3	20.15	8.37	0.95	3.60	3.02	1.09	0.06	1.13	0.14	0.53
88–90	dam construction		50.7	43.5	52.7	3.8	20.85	8.09	0.94	3.41	3.08	1.01	0.05	1.25	0.14	0.50
90–92		4 ± 0.4	55.9	46.4	50.2	3.4	20.84	7.95	0.94	3.32	3.14	0.99	0.05	1.25	0.14	0.47
92–94			27.1	25.5	69.8	4.7	20.83	7.78	0.94	3.24	3.07	0.99	0.05	1.24	0.13	0.46
94–96			25.8	24.8	70.1	5.1	19.04	8.66	1.05	4.05	2.99	1.19	0.08	0.98	0.15	0.57
96–98			28.7	28.4	66.7	4.9	19.03	8.67	1.06	4.19	2.98	1.21	0.08	0.96	0.16	0.59
98–100			54.7	45.2	50.8	3.9	20.37	8.16	0.94	3.51	3.00	1.01	0.06	1.16	0.14	0.54
100–102		6 ± 0.6	42.7	39.5	56.5	3.9	21.26	7.79	0.91	3.22	2.97	0.92	0.06	1.31	0.16	0.50
102–104			26.0	26.2	69.2	4.6	21.14	8.01	0.86	3.30	2.95	0.93	0.07	1.26	0.17	0.47
104–106			20.8	19.0	76.1	4.9	18.74	8.67	1.04	4.24	2.91	1.21	0.09	0.92	0.16	0.59
106–108			20.5	19.0	76.1	4.8	18.14	8.72	1.09	4.52	2.84	1.25	0.11	0.88	0.19	0.60
108–110			33.3	34.7	61.5	3.8	18.46	8.60	1.02	4.26	2.82	1.18	0.10	0.96	0.20	0.58
110–112		9 ± 0.5	31.3	32.0	64.2	3.8	19.27	8.34	0.96	3.96	2.81	1.08	0.09	1.15	0.21	0.55
112–114			25.3	25.9	70.0	4.1	17.44	8.26	0.94	4.41	2.61	1.07	0.15	0.91	0.31	0.55
114–116			18.0	13.4	81.8	4.8	18.40	8.32	1.04	4.44	2.75	1.13	0.16	0.96	0.26	0.56
116–118			15.4	11.4	83.0	5.5	18.16	8.34	0.95	4.48	2.68	1.10	0.17	0.93	0.30	0.55
118–120			15.8	12.5	82.6	4.9	17.06	8.91	0.90	4.80	2.56	1.21	0.16	0.75	0.31	0.56
120–122		8 ± 0.9	16.7	13.3	82.0	4.7	17.69	8.54	0.80	4.55	2.43	1.13	0.16	0.72	0.33	0.55
122–124			19.8	16.9	79.0	4.1	17.10	8.64	0.76	4.58	2.43	1.17	0.17	0.68	0.31	0.54
124–126			19.4	17.3	77.9	4.8	17.46	8.58	0.79	4.61	2.39	1.11	0.17	0.72	0.35	0.55
126–128			59.2	48.9	48.0	3.1	17.42	8.45	0.84	4.28	2.41	1.08	0.10	0.80	0.26	0.57
128–130			140.9	69.8	28.2	2.0	18.75	8.99	0.93	4.50	2.76	1.18	0.09	0.96	0.21	0.58
130–133		4 ± 0.6	120.9	66.2	31.7	2.0	18.42	9.39	0.85	4.97	2.81	1.27	0.10	0.81	0.24	0.55
133–134			119.9	67.6	30.3	2.1	17.68	9.64	0.83	5.27	2.80	1.32	0.11	0.64	0.24	0.60
134–136			100.4	61.4	36.2	2.3	18.46	9.20	0.88	4.85	2.77	1.23	0.10	0.82	0.26	0.59
136–138			284.4	88.4	10.8	0.8	17.45	9.75	0.87	5.14	2.77	1.30	0.10	0.68	0.23	0.60

TC	TS	Ba	Hf	La	Rb	Sm	Th	U	Zr	As	Bi	Cd	Cr	Cu	Hg	Mo	Ni	Pb	Sb	Sn	W	Zn
%	%	ppm	ppm	ppm	ppm	ppm	ppm	ppm	ppm	ppm	ppm	ppm	ppm	ppm	ppm	ppm	ppm	ppm	ppm	ppm	ppm	ppm
5.58	0.27	531	3.2	34.8	191.3	5.72	13.1	7.6	114.8	44.7	2.1	1.7	116	52.3	0.22	0.9	39.4	87.8	1.0	18	5.6	217
3.70	0.11	589	3.8	38.0	212.8	6.33	13.8	7.5	139.3	29.4	1.9	1.5	130	45.3	0.19	0.8	42.0	72.7	0.6	15	5.5	215
3.99	0.07	573	4.7	39.8	207.1	6.62	15.8	7.3	174.7	27.5	2.2	1.5	130	50.2	0.23	0.8	41.3	69.0	0.7	18	6.4	206
3.22	0.08	588	4.0	36.8	222.5	6.19	12.4	6.6	151.9	21.5	1.3	0.9	144	41.6	0.12	0.8	46.9	51.1	0.4	13	4.8	168
4.51	0.07	594	4.7	37.9	214.9	6.30	13.4	7.1	171.1	23.0	1.6	1.4	144	48.7	0.18	0.9	44.7	61.5	0.5	17	5.6	199
5.09	0.1	573	5.8	38.7	202.7	6.63	15.3	7.8	191.1	28.8	2.3	2.0	130	54.9	0.26	1.1	43.8	72.5	0.8	20	6.6	221
5.23	0.11	597	6.5	44.3	183.0	7.27	19.8	8.3	236.2	36.9	3.7	2.6	116	63.3	0.43	1.2	41.6	84.8	1.2	22	8.3	257
5.56	0.11	608	6.8	45.5	176.7	7.46	20.0	8.2	229.3	38.2	4.3	2.1	103	66.2	0.37	1.2	38.6	88.3	1.2	23	8.1	269
5.41	0.12	626	5.8	45.2	187.3	7.40	21.5	8.7	211.5	41.4	4.3	2.2	103	61.7	0.40	1.1	37.6	92.9	1.2	21	8.5	254
n.d.	n.d.	n.d.	n.d.	n.d.	n.d.	n.d.	n.d.	n.d.	n.d.	n.d.	n.d.	n.d.	n.d.	n.d.	n.d.	n.d.	n.d.	n.d.	n.d.	n.d.	n.d.	n.d.
<d.l.	<d.l.	567	3.4	38.8	183.4	6.37	16.6	8.0	110.8	42.2	3.7	2.1	123	55.7	0.29	0.8	40.9	101.8	1.0	17	6.1	243
5.94	0.25	561	3.9	39.7	179.2	6.57	17.4	9.1	133.2	51.1	3.2	1.7	116	59.2	0.29	0.9	40.0	96.2	1.0	15	6.2	227
4.55	0.24	598	3.6	39.6	200.6	6.50	17.4	8.3	128.1	51.4	2.4	1.8	123	55.1	0.28	1.0	43.1	86.8	1.0	17	6.4	215
3.79	0.14	618	4.1	40.2	213.0	6.59	18.6	8.1	141.5	40.6	2.1	1.7	123	52.6	0.30	0.8	43.6	79.9	1.0	17	6.6	214
3.30	0.09	603	4.4	39.6	248.2	6.48	16.3	8.2	150.4	35.1	1.6	1.5	123	50.4	0.25	0.8	46.7	72.0	0.7	19	6.7	204
3.01	0.09	588	4.5	38.8	252.4	6.67	16.0	7.5	153.5	31.9	1.5	1.1	123	44.6	0.22	0.9	46.3	61.1	0.7	20	6.3	169
4.36	0.11	656	5.5	43.7	239.4	7.20	17.5	8.4	193.8	33.1	1.7	1.9	144	54.5	0.34	1.1	49.9	73.9	0.9	24	7.5	209
4.47	0.11	658	6.3	44.2	233.1	7.42	19.2	8.5	212.0	36.6	1.9	2.6	144	63.5	0.49	1.2	54.7	82.9	1.0	26	8.9	247
4.76	0.13	665	6.9	45.9	223.2	7.70	23.0	9.0	236.9	38.9	1.9	2.7	151	70.2	0.48	1.4	55.5	90.0	1.1	26	9.5	278
5.07	0.13	682	8.2	52.4	217.6	8.45	23.7	9.7	275.1	41.3	1.8	3.2	151	73.5	0.53	1.5	56.8	97.2	1.3	27	10.2	293
4.68	0.11	659	8.9	53.7	215.4	8.73	25.7	9.7	297.4	38.3	1.8	2.9	137	69.2	0.47	1.4	52.8	89.4	1.1	23	9.6	275
3.47	0.09	702	13.6	70.2	211.8	11.18	35.2	10.6	471.9	31.2	1.3	2.2	123	55.3	0.38	1.1	44.9	74.5	1.1	20	9.0	229
5.00	0.13	677	7.8	51.7	211.2	8.45	24.8	9.6	277.7	38.1	1.6	2.8	144	76.4	0.46	1.5	54.2	93.7	1.2	25	10.8	289
5.35	0.13	692	6.7	46.9	222.0	7.71	21.6	9.5	227.0	43.3	1.8	3.2	144	83.9	0.53	1.5	56.5	103.4	1.2	25	10.3	326
5.17	0.12	633	4.4	41.7	221.1	6.56	19.3	9.1	150.9	44.1	1.6	2.2	116	75.5	0.42	<d.l.	53.5	95.8	1.1	19	8.0	291
<d.l.	<d.l.	554	3.5	37.4	212.9	5.99	15.9	9.5	113.0	46.5	1.3	1.3	96	68.9	0.27	1.1	51.8	95.3	1.1	15	6.1	229
4.36	0.14	664	3.8	41.6	255.9	6.65	18.3	8.9	125.7	37.9	1.4	1.6	109	57.5	0.27	1.0	47.2	90.2	1.2	17	6.7	243
4.15	0.18	646	4.6	42.9	257.2	6.79	18.5	9.3	149.1	42.7	1.5	1.5	123	60.9	0.23	0.9	52.2	90.1	1.1	16	6.9	227
4.74	0.23	651	3.8	42.8	237.6	6.88	17.9	9.2	139.3	49.3	1.5	2.6	151	66.9	0.31	1.5	63.0	97.6	1.0	19	7.3	262
3.49	0.09	697	4.5	41.9	263.5	6.75	18.9	8.2	161.2	29.9	1.6	2.0	151	53.2	0.30	0.9	52.8	79.3	0.5	21	7.1	249
5.11	0.13	691	5.0	43.6	232.5	7.51	19.8	9.3	187.8	38.6	1.9	3.8	185	73.8	0.53	1.7	64.1	95.7	1.1	31	10.1	325
5.67	0.15	721	6.5	43.2	221.3	7.42	20.3	9.6	202.1	44.4	2.1	4.7	192	86.2	0.70	2.0	66.9	107.1	1.1	34	10.8	369
5.44	0.24	622	3.6	40.1	244.7	6.56	16.7	10.0	124.5	45.1	2.0	2.9	267	68.0	0.32	1.2	65.8	103.9	0.7	27	7.3	282
4.77	0.12	678	3.9	41.0	244.9	6.82	17.4	9.6	134.4	39.0	2.0	3.7	328	64.6	0.30	1.1	57.1	101.5	0.6	31	7.7	305
3.79	0.1	669	4.8	42.9	242.8	7.26	19.7	9.3	153.7	38.6	1.5	3.3	144	60.8	0.33	1.0	50.0	86.8	1.2	24	8.6	292
4.15	0.11	661	3.8	41.7	238.7	6.73	19.3	10.0	135.1	42.6	1.5	2.9	144	63.4	0.31	0.8	53.0	100.8	1.3	20	8.3	311
4.58	0.23	677	3.9	41.4	228.5	6.76	20.7	10.1	133.7	50.3	1.5	3.3	151	65.1	0.31	<d.l.	63.9	114.3	0.8	22	8.6	287
4.70	0.17	701	4.6	44.0	234.4	7.14	21.0	10.6	138.8	49.7	1.6	3.7	157	70.7	0.33	1.0	64.9	116.8	0.7	23	8.4	309
4.24	0.17	696	4.4	44.7	236.7	7.29	21.2	10.1	155.7	49.2	1.8	4.7	178	65.3	0.30	0.9	71.7	137.1	0.6	23	8.6	282
4.20	0.14	692	4.1	42.7	241.2	7.10	21.0	10.4	144.0	50.6	1.8	4.2	219	71.8	0.33	<d.l.	63.6	119.1	0.9	26	8.0	304
3.41	0.17	710	4.8	43.9	245.4	7.24	20.8	8.9	167.8	47.6	1.8	6.1	198	61.8	0.51	1.4	66.1	102.1	1.1	27	8.3	295
4.64	0.19	718	7.1	46.3	222.9	7.81	22.3	10.1	237.2	54.6	2.5	10.5	246	73.2	0.46	1.8	81.2	108.6	0.8	38	10.7	382
4.27	0.24	707	10.5	59.1	217.6	10.03	28.4	10.3	371.3	39.8	2.2	3.1	144	46.1	0.36	1.3	55.7	69.7	1.0	33	11.8	194
3.90	0.09	708	10.9	59.5	224.6	10.09	30.7	9.6	379.1	28.7	1.9	1.7	123	38.1	0.36	1.1	40.8	58.9	0.8	27	9.6	152
3.28	0.07	729	10.9	59.8	219.1	10.28	31.9	9.0	387.5	25.9	1.6	1.8	130	33.2	0.22	1.2	37.9	53.9	1.1	23	9.4	149
2.99	0.06	754	10.5	57.2	219.4	9.42	29.8	9.0	364.2	26.2	1.7	1.9	116	32.6	0.20	1.1	39.5	53.0	0.9	31	9.3	156
3.78	0.08	727	9.9	54.4	222.6	9.33	29.5	8.8	347.7	24.8	1.6	1.7	116	30.5	0.18	1.2	37.7	48.9	0.8	19	7.9	146
3.93	0.09	733	8.9	52.2	233.9	8.68	25.6	9.4	307.1	33.0	2.6	2.7	151	42.6	0.33	1.2	43.4	65.8	0.8	29	9.7	178
3.91	0.08	729	8.6	50.2	236.2	8.65	25.4	9.5	318.4	34.5	2.5	3.0	157	46.1	0.37	1.2	46.7	68.5	0.9	31	9.7	188
3.93	0.07	758	11.2	61.8	225.3	10.10	30.7	9.6	397.7	30.3	2.0	2.4	137	37.2	0.27	1.2	42.4	61.9	1.0	23	9.0	170
3.02	0.06	675	11.6	68.7	196.9	11.39	33.8	10.1	401.3	31.2	1.5	3.2	144	36.0	0.41	1.5	48.0	60.2	1.1	19	8.2	194
3.83	0.07	661	9.0	57.4	201.3	9.35	27.4	8.8	335.0	31.5	1.7	4.7	151	40.1	0.57	1.0	51.3	62.3	1.0	22	8.6	217
3.60	0.06	636	8.2	47.0	224.7	8.11	23.3	8.8	281.4	34.7	2.5	3.0	164	45.8	0.46	1.2	52.4	72.0	1.0	28	8.3	198
4.76	0.07	671	7.6	46.6	223.2	8.03	23.0	9.1	253.9	43.2	3.2	5.7	212	61.7	0.49	1.5	64.0	90.0	1.5	36	10.2	267
4.52	0.07	655	7.9	49.3	216.9	8.46	25.5	9.2	274.0	39.9	2.8	6.0	198	60.3	0.59	1.6	67.8	88.3	1.4	30	9.0	275
5.16	0.08	704	9.2	51.1	206.0	9.02	25.6	9.0	322.3	38.5	2.6	5.6	212	59.7	0.55	1.8	71.8	87.1	1.7	29	10.1	275
6.74	0.09	743	7.7	50.6	207.9	8.56	24.5	10.3	259.7	56.3	3.5	13.2	301	92.3	0.61	2.1	104.3	125.1	1.6	37	12.4	474
5.23	0.11	707	8.9	49.4	215.6	8.38	24.1	9.4	305.6	40.8	3.1	10.3	260	77.4	0.50	2.0	100.4	106.3	1.5	40	11.8	386
5.33	0.12	740	8.7	52.4	213.4	9.05	24.7	9.9	298.9	45.8	3.6	14.6	281	92.7	0.64	2.4	114.8	125.1	1.5	44	14.5	474
5.79	0.14	749	5.6	43.1	222.6	7.51	19.9	9.5	201.4	56.3	4.2	18.4	328	113.5	0.79	2.8	155.7	147.9	1.9	53	15.0	588
<d.l.	<d.l.	655	6.1	44.2	212.5	7.72	20.0	8.7	219.8	43.5	3.3	13.2	267	86.6	0.51	1.7	121.1	125.1	1.3	37	11.1	454
5.50	0.12	645	5.4	43.1	220.9	7.58	20.6	8.8	193.3	46.1	3.2	14.1	267	92.1	0.58	1.6	121.6	127.0	1.1	38	10.5	463
5.23	0.18	647	6.1	45.8	213.9	7.88	22.5	9.1	209.6	48.6	3.4	13.7	267	85.7	0.49	1.6	167.3	132.3	1.3	35	10.3	461
5.43	0.1	711	6.5	44.1	209.0	7.68	21.5	10.8	214.4	52.4	3.4	13.0	335	81.0	0.49	2.1	145.2	131.1	1.4	37	9.8	460
3.99	0.08	753	7.7	49.4	211.4	8.46	23.6	10.4	263.2	45.4	3.8	5.6	287	65.6	0.47	<d.l.	98.7	120.8	1.9	33	9.8	321
<d.l.	<d.l.	710	6.2	47.3	228.5	7.90	23.6	10.0	218.3	36.9	4.1	4.4	267	55.8	0.30	1.9	97.5	111.5	1.1	32	9.9	264
3.13	0.04	690	8.6	56.4	237.7	9.56	30.1	10.8	284.4	21.8	1.9	2.4	274	30.8	0.32	<d.l.	56.4	57.5	0.9	35	9.6	166
3.63	0.04	721	9.5	58.2	227.3	9.74	30.0	11.2	323.5	39.8	3.6	3.7	267	50.7	0.47	<d.l.	96.4	98.6	1.4	33	10.4	261
4.51	0.07	745	7.3	50.5	230.7	8.52	25.6	10.3	261.8	51.4	4.1	7.1	335	62.2	0.46	<d.l.	108.4	116.1	1.5	40	13.0	335

138–140		179.8	78.2	20.4	1.3	18.18	10.13	0.85	5.52	3.00	1.44	0.12	0.62	0.23	0.55
140–142	4 ± 0.3	236.7	83.2	15.6	1.2	18.02	9.78	0.90	5.42	2.92	1.34	0.12	0.70	0.24	0.61
142–144		155.4	71.2	27.0	1.8	17.36	9.65	0.92	5.22	2.75	1.27	0.09	0.67	0.22	0.60
144–146		194.7	80.1	18.6	1.3	17.29	9.50	0.86	5.38	2.80	1.31	0.13	0.64	0.26	0.56
146–148		187.8	79.0	19.7	1.4	16.51	9.41	0.82	5.45	2.71	1.28	0.13	0.56	0.28	0.55
148–150	7 ± 0.5	188.0	79.8	19.0	1.2	17.08	9.52	0.84	5.23	2.74	1.25	0.12	0.65	0.22	0.56
150–152		159.3	73.0	25.4	1.6	18.07	9.26	0.87	4.92	2.82	1.22	0.12	0.79	0.23	0.55
152–154	6 ± 0.7	79.8	56.6	40.8	2.7	18.26	9.39	0.90	4.82	2.85	1.23	0.09	0.84	0.20	0.57
					d.l.	*0.01*	*0.01*	*0.01*	*0.03*	*0.01*	*0.01*	*0.01*	*0.01*	*0.01*	*0.01*
					Preindustrial concentrations	26.37	8.45	1.57	4.27	2.35	0.94	0.08	0.96	0.13	0.75

they are involved in the same domain in the C–M diagram, and the vertical grain-size sorting shows a similar hysteresis (Fig. 3.).

3.1.2. Stratigraphic evidence of flood sequences

A detailed sedimentological analysis of the upper unit of the core allows us to enhance the sediment layers that settled in a lacustrine context and possibly came from events with important sedimentary loads. The coarser and lighter layers at the 58–64 cm, 30–50 cm and 6–19 cm depths look like turbidites, as they are described in lakes (Giovanoli, 1990; Sturm and Matter, 1978) and reservoirs (Ambers, 2001), when associated with important flood events and massive material transport. During important discharge events entering the reservoir, the riverine sediment load is transported according to the grain-size of the particles, river flow density and water density stratification. The coarsest sediments are mainly deposited in the reservoir delta and the residual flow generates fine sediment-laden under- and overflows deposited further in the reservoir floor.

For these turbidite-like layers, well-marked D_{50} and D_{90} patterns in the C–M diagram (total grain-size hysteresis for the 58- to 64-cm and 30- to 50-cm-deep layers and a partial hysteresis for the 6- to 19-cm sequence) can be associated with underflow-related depositional processes (Gilli et al., 2013; Giovanoli, 1990). These flood sequences would correspond to the most important events since the dam began operation in 1984, i.e., the 58- to 64-cm interval to the 1996 flood, the 30- to 50-cm interval to the 2003 flood and the 6- to 19-cm interval to the 2008 flood. In particular, this 2008 flood event was not managed like the two previous ones. The dam gates usually open gradually to regulate downstream runoff according to the upstream flood hydrogram. However, in 2008, the reservoir water level was already high before the flood event and the dam gates were opened the same time the flood began (H. Xhaard, EPL, pers.com.). This dam management may be related to the incomplete hysteresis in the 6- to 19-cm interval (D_{50} and D_{90} are only correlated up to 14 cm deep in a decreasing trend, Fig. 2). In unit 2, which was deposited during the reservoir water infilling, the 104- to 128-cm interval could correspond to the major 1983 flood with a greater than 20-year flood average daily outflow.

3.2. Age model definition

3.2.1. ^{137}Cs dating

The ^{137}Cs activity shows a well-marked maximum (124.2 ± 1.4 Bq·kg^{-1}) at 80–82 cm (Table 1). This ^{137}Cs peak is preceded by ϒ activities between 5.6 ± 0.7 and 19.6 ± 1.2 Bq·kg^{-1}. The bottom of the lacustrine sedimentary record at 82–84 cm is assumed to be synchronous with the Villerest Dam's full operation beginning in 1984. In these circumstances, the ^{137}Cs peak can correspond to the C-NPPD fallout in 1986. The detection of some ^{137}Cs in units 2 and 3, ranging between 4.1 ± 0.3 and 9.2 ± 0.5 Bq·kg^{-1} (Table 1), indicates that these deposits belong to the post-1950 period. Nonetheless, the post-depositional mobilization of the ^{137}Cs during diagenesis and the resulting down migration of this radionuclide in the sedimentary column could disturb the dating (Benoit and Rozan, 2001; Smith et al., 2000). In particular, unit 2 is associated with the reservoir water infilling. According to the dam managers, the water infilling period lasted from the end of the dam's construction in 1983 to 1984. The

heavy aggradation rate of this unit should reflect important local sedimentary inputs in the downstream part of the reservoir during the water filling operation. Two hypotheses can be formed regarding the sediment origin in unit 3: (i) these sediments were part of a former river bank of the Loire River before the dam's construction, and the absence of the NWT maximum fallout (1964 ^{137}Cs peak) is then related to sediments younger than 1964; or (ii) the sediments from unit 3 could have been partly reworked during the dam construction starting in the late 1970s. The lack of the 1964 ^{137}Cs peak would then be due to a sediment hiatus in the bottom unit 3 as parts of these channel sediments were scrabbled and exported during the dam construction. The sediments from unit 3 could not have been more precisely dated.

3.2.2. Age model calculation

To take into account the temporal variations in the sedimentation processes, the flood events' influence on sedimentary infill and the compaction variations with depth during coring, an age model was precisely built on the calculation of mass accumulation rates (MAR, kg·m^{-2}·y^{-1}; Van Metre et al., 2004) using the two absolute depth–date markers and flood markers.

This age model is first based on the dry mass parameter (DM; kg·m^{-2}), calculated as follows:

$$DM = (1-n) \cdot DS \cdot Th \tag{1}$$

with n as the porosity (%; the volume of water contained in a well-known volume of fresh sediments), DS as the apparent density of the sediments (g·m^{-3}; the dry mass material contained in the defined volume) and Th as the thickness of the sampled layer (m).

The MAR is then expressed between each date-bounded interval by dividing the cumulative dry mass (cum) with the time interval (TI; year) as follows:

$$MAR = cum/\text{TI}. \tag{2}$$

Therefore, the corresponding age of the sediment (Date) at a level i is calculated as follows from the top of the core (=coring date; 2010 in the study case) to the first time marker:

$$Date_i = \text{coring date} - (cum/MAR). \tag{3}$$

For sediment layers j older than the first time marker i, Eq. (4) is then applied:

$$Date_j = \text{marker date}_i - \left(cum_j - cum_i\right)/MAR_j. \tag{4}$$

The cumulative dry mass slope varies according to the depth from 1.9 kg·m^2·cm in unit 1 to 4.2 kg·m^2·cm in unit 2 and 8.0 kg·m^2·cm in unit 3 (Fig. 4). These variations correspond to the 3 aforementioned sediment units. In particular, unit 1 shows light variations in the cumulative dry mass slope associated with the 3 identified major floods in the sediment sequence. The MAR was then adjusted in the upper unit 1: (i) when considering the whole unit 1 between the 1984 and 2010 depth–date markers, the MAR reaches 5.8 kg·m^{-2}·y^{-1}; (ii) when taking into account each flood sequence (1996, 2003 and 2008) as a depth–date marker, the MAR fluctuates between 2.0 and 3.0 kg·m^{-2}·y^{-1}

3.70	0.06	776	6.3	46.9	241.0	7.94	23.9	10.5	207.7	49.3	5.0	4.4	308	76.0	0.41	<d.l.	91.2	123.0	1.3	42	10.8	377
4.00	0.1	865	7.8	52.7	235.4	8.78	25.9	11.1	278.1	55.9	4.7	5.3	308	51.4	0.33	<d.l.	157.6	109.5	1.3	40	11.2	291
5.41	0.07	788	8.7	56.9	230.2	9.40	27.0	11.4	321.2	56.9	6.9	6.6	383	102.2	0.42	<d.l.	126.7	139.8	1.6	46	13.0	460
4.32	0.06	756	8.6	58.2	236.2	9.62	28.0	11.3	308.0	48.7	9.5	6.5	342	63.1	0.35	<d.l.	97.2	128.5	1.3	51	12.3	299
5.01	0.05	744	6.3	47.6	242.2	8.16	23.4	11.2	214.6	44.5	9.6	6.5	363	63.3	0.38	<d.l.	96.7	124.4	1.3	55	12.5	317
5.21	0.08	753	5.3	45.5	241.4	7.99	22.7	10.7	185.1	38.9	9.3	6.5	397	61.4	0.38	<d.l.	96.8	116.4	1.5	53	14.4	270
4.04	0.05	738	7.2	47.5	233.0	8.20	22.4	9.4	244.6	38.5	7.3	4.1	308	54.8	0.36	<d.l.	92.5	97.1	1.2	48	12.6	242
<d.l.	<d.l.	753	9.2	55.7	230.5	9.64	27.2	10.6	325.4	48.5	8.8	5.6	294	93.4	0.42	2.2	91.3	123.6	1.4	48	13.1	304
0.02	*0.02*	*1*	*0.1*	*0.1*	*0.1*	*0.05*	*0.2*	*0.1*	*0.1*	*0.5*	*0.1*	*0.1*	*14*	*0.1*	*0.01*	*0.1*	*0.1*	*0.1*	*0.1*	*1*	*0.5*	*1*
1.15	n.d.	661	11.7	64.1	165.0	10.065	25.1	8.2	405.5	19.6	0.7	0.4	99	20.0	0.02	0.4	28.4	34.7	0.4	8	6.0	94

(Fig. 4). These three flood events highly contribute to the sediment budget as they correspond to 43% of the settled sediments since the beginning of the dam's operation (total of 151.4 kg·m^{-2} of trapped sediments, calculated by cumulating DM over unit 1) with 8.3, 41.0 and 16.3 kg·m^{-2} of material, respectively, instantly deposited (5.5, 27.1 and 10.8% of the total sedimentary infill since 1984). Such an influence of large flood events on the aggradation rate has been highlighted for flood-control reservoirs built in a mountain context (low-order stream, steep slope and storm influenced climate, Ambers, 2001), but never for high-order stream draining large watersheds as in the studied reservoir.

3.3. Temporal dynamics of the trace element contaminations

3.3.1. Influence of flood events in the registered enriched TE trends

The sedimentological analysis of the depositional conditions highlights the non-linear aggradation rate during the sedimentary infilling of the Villerest reservoir caused by flood event deposits. According to the detailed age model, the temporal variations in the trace element contents could then be described in the upper unit of the core. In a sedimentary archive, the trace element concentrations can vary with depth by several orders of magnitude according to the temporal variations in both natural and anthropogenic inputs and, to a lesser extent, by chemical remobilization processes. Enrichment factors (EF) were chosen to describe the temporal dynamics of selected trace elements presenting an anthropogenic influence in the studied sediment core. They were calculated in the <63 μm fraction using the natural geochemical reference of the entire Loire basin (Grosbois et al., 2012; Table 1).

Trace elements such as *Ba*, *La*, *Th*, *Hf*, *Sm*, *U* and *Zr* present EF close to 1. These trace elements are usually considered as tracers of detrital sources as they are specifically associated with mineral hosts. *Zirconium* and *Hf* can be enriched in sediments containing zircons, *barium* in the presence of barite, and *rare earth elements* in phosphates and Ti-bearing heavy minerals (Dill, 2010). Some other trace elements such as *Cu*, *Sb*, *Sn*, *Pb* and *Zn*, which are potentially associated with diffuse and/or local anthropogenic sources (i.e., Callender, 2003; Kabata-Pendias, 2000; Pacyna and Pacyna, 2001), present a light anthropogenic influence in the studied sediments as their EFs range from 2 to 4. A temporal decline is not clearly expressed, and flood sequences are seemingly more impacted than others (Table 1). The most enriched trace elements (EF >6) in the studied area are *Bi*, *Cd* and *Hg*. Even if these trace elements are always enriched throughout unit 1, their EF values appear higher in flood sequences, similar to *Cu*,
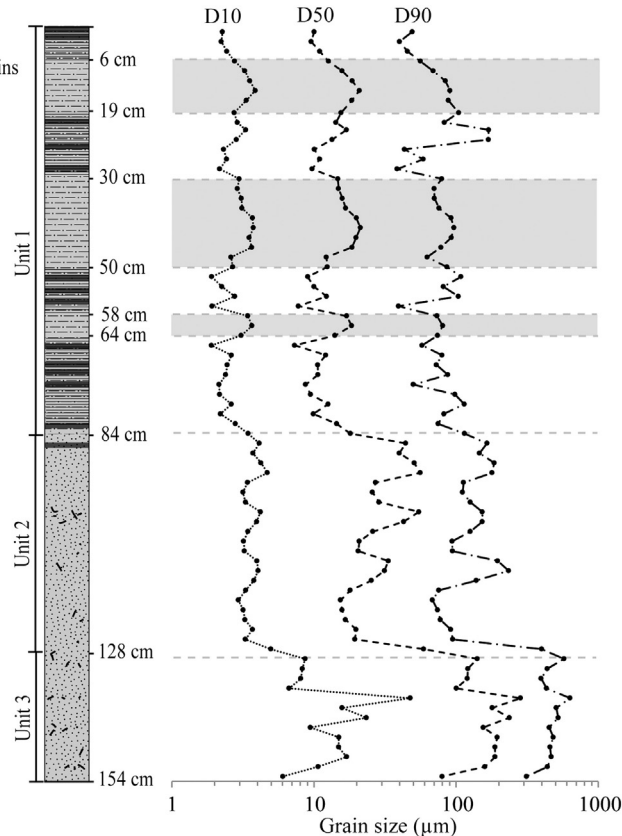
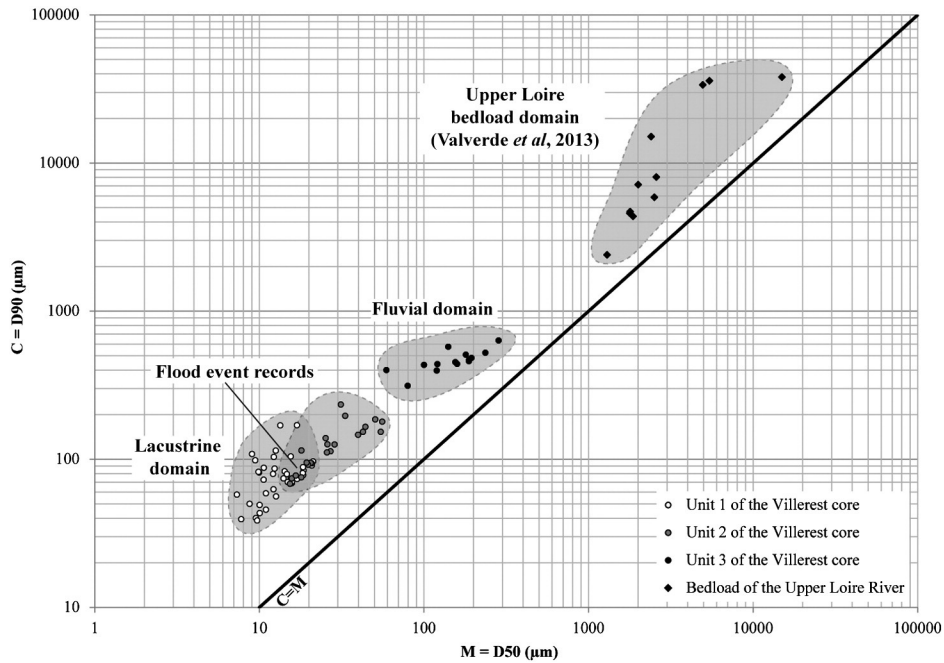**Fig. 2.** Sedimentary log with grain-size parameters (D$_{10}$, D$_{50}$ and D$_{90}$) in each 2-cm thick layer.

Fig. 3. The C–M diagram for the 3 core units and associated depositional condition domains according to Passega (1957, 1964).

Sb, *Sn*, *Pb* and *Zn* (Fig. 5; Table 1), with enrichment maxima up to 6.8 for *Bi*, 15.5 for *Cd* and 34.2 for *Hg*.

These flood events carry solid trace element-rich materials provided by various natural (*Ba*, *Hf*, *La*, *Sm*, *Th*, *U*, *Zr*) and anthropogenic sources. The temporal dynamics of the TE concentrations depend on the relative importance between mechanisms such as coarse non-impacted particle dilution, trace element chemical remobilization and anthropogenic metal sources mobilized during a flood event. In the studied flood sequences, the most enriched trace elements are *Bi*, *Cd* and *Hg*, and the flood periods represent the highest levels of contamination throughout
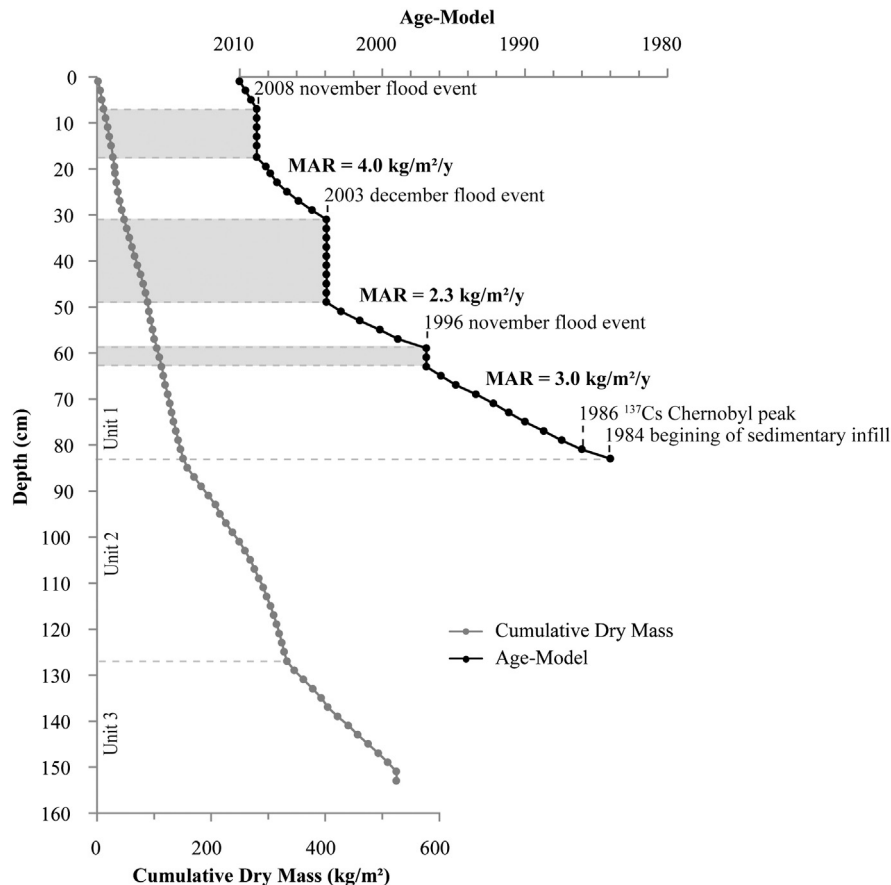
Fig. 4. The age model with the cumulative dry mass in the 3 sedimentary units and the mass accumulation rates in unit 1 from the core.

the entire 1984–2010 period. Hence, additional anthropogenic sources were solicited or enhanced during these specific hydrological events. This type of enrichment maximum associated with particle transport during a flood event has been already observed for suspended matter fractions in Coynel et al. (2007) and for sediment archives in Bábek et al. (2011), for instance.

In geochemical studies, age models are usually conducted with continuous sedimentation rates (e.g., Audry et al., 2004; Grosbois et al., 2012; Grousset et al., 2001; Le Cloarec et al., 2011). In the Villerest reservoir context, taking into account the flood sequences and MAR variations in the definition of the age model induces large differences. The 2 absolute depth–date markers available in this study (1986 for the 80–82 cm deep layer and 2010 for the 0–2 cm deep layer) allow us to calculate a linear sedimentation rate equal to 3.4 cm·y^{-1}. With this first age model, the flood sequences at the 58–64 cm, 30–50 cm and 6–19 cm depths are wrongly dated to the early 1990s, 1995–2001 and 2005–2009 periods, respectively. When considering this continuous sedimentation rate, the flood sequences are also wrongly associated with highly impacted periods (Fig. 5).

3.3.2. Chemical characteristics of detrital material inputs during flood events

The high analysis resolution for the 2003 (n = 10 analyzed 2-cm thick layers) and 2008 (n = 6) flood events was enough to adequately describe the chemical variations during such a hydrological event record in the studied core. Such an approach was not made for the 1996 flood record as only three 2 cm-thick sediment layers were made, nor for the 1983 flood as this flood occurred during the dam's water filling conditions.

For the major element patterns during the 2003 flood, the *silicon* content begins to increase to a maximum peak at 42–44 cm depth (27.4% Si). The sand percentage and D$_{50}$ also increase, but their maxima are present at 40–42 cm depth (Fig. 6a) and define the rising phase of the 2003 flood (named after stage I), as already described by Alvarez-Iglesias et al. (2007) and Bábek et al. (2011). *Sodium* and the *K/Rb* ratio follow this *Si* pattern, similar to detrital trace elements such as *Ba, La, Th, Hf, Sm, U* and *Zr* (Fig. 6a). In the meantime, elements such as *Al, Fe, Mg, TC, TS* and, to a lesser extent, *Ti* and *Mn* first decrease during stage I with well-marked depleted layers at 42–44 cm depth (Fig. 6a). The *Si/Al* ratio then presents a well-defined bell-curve with a maximum centered on the 42–44 cm layer (Fig. 6a). A slight temporal decoupling is

then observed between the *Si/Al* ratio and grain-size parameters. As the *Si/Al* ratio is usually used as a mineralogical tracer (Alvarez-Iglesias et al., 2007; Bouchez et al., 2011; Chen and Kandasamy, 2007), stage I can be related to the solid transport of an important input of detrital material. The increase in grain-size, following the *Si/Al* variations in stage I, emphasize the coarse characteristics of this detrital material during the flood rising phase (Walling et al., 1997). However, the temporal decoupling between the geochemical detrital signature and grain-size parameters could be linked to the time gap between the runoff and bedload mobilization during the clockwise hysteresis response of a flood hydrogram in the Loire River system, as shown by Claude et al. (2012). The decrease in *Fe, Mg, Ti, TC* and *TS* at the same time can be related to a dilution by coarse and Si-rich detrital inputs.

In the flood sequences, a second stage can be delineated (Stage II in Fig. 6) that is associated with the grain-size decrease. Ratios such as *Si/Al* and *K/Rb* and the detrital trace element contents decrease at the same time as D$_{50}$ and the sandy fraction. The *Manganese, TC* and *TS* contents start to increase (maximum at 38–40 cm for the 2003 flood) before their contents decrease until the end of the flood (from 38 to 30 cm deep). At the same time, the percentage of clayey fraction starts to increase (from 4.1% to 5.6%) and is associated with a well-marked upward increase in *Al, Fe, Mg, Ca* and *Ti* content. The depth level, associated with the concentration maxima, then shifted for the 2 different element groups at 42–44 cm for the *Si/Al, Na,* and *K/Rb* maxima and at 32–34 cm for the *Al, Fe, Mg, K,* and *Ti* maxima. Stage II can be related to the end of the flood hysteresis, when underflow declined and the finest sediments in the suspension present in the water column began to settle. The increase in major elements such as *Al, Fe, Mg, Ca* and *Ti* indicates that these fine particles may be associated with clay and (Fe, Ti) oxyhydroxide transport.

The 2008 flood's sedimentary record is less well-defined relative to the dam's specific management when the Villerest Dam was transparent during the flood rising phase. The stage I sand percentage, defined by D$_{50}$, and *Si/Al* increase in the 2003 flood do not seem to be as well registered for the 2008 flood. The increasing sand percentage phase is missing (Fig. 6b), and the *sodium* and *Si/Al* and *K/Rb* ratios only present steady levels from 19 to 14 cm deep. At the same time, the *Fe, Ti* and *Mg* concentrations are the lowest during the 2003 flood. Stage II's decreasing *Si/Al,* D$_{50}$ and sand percentage are similar in both flood registered sequences with a well-marked increase in the Fe content and clay percentage.
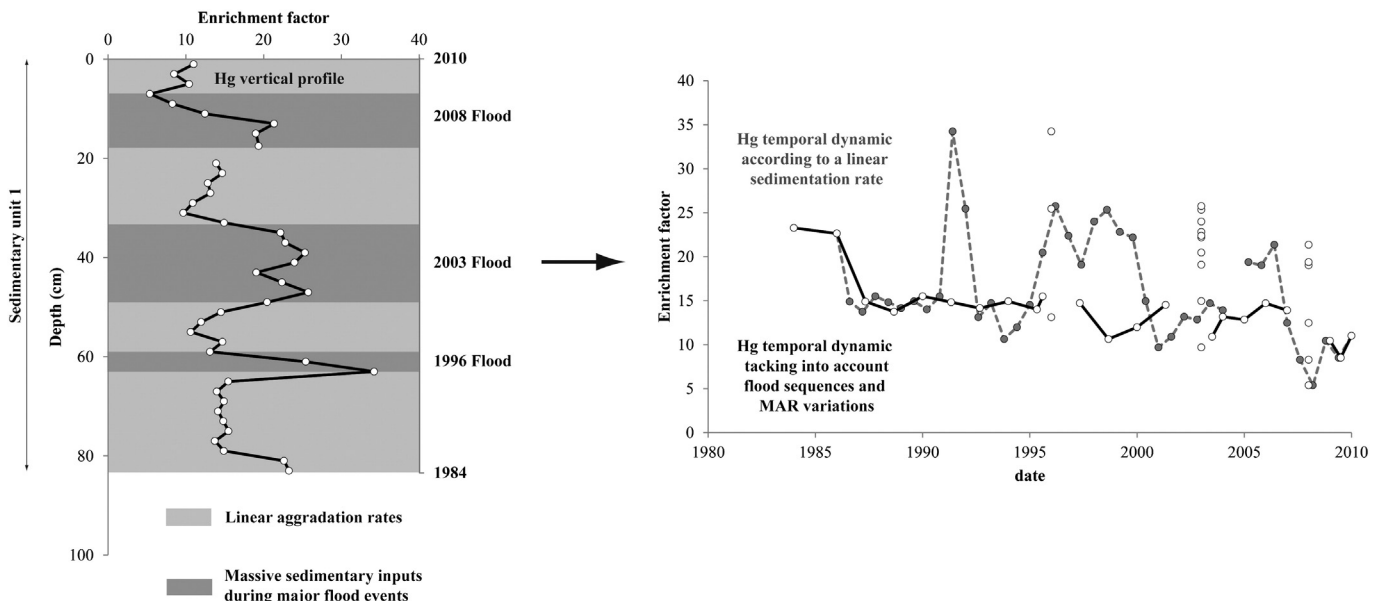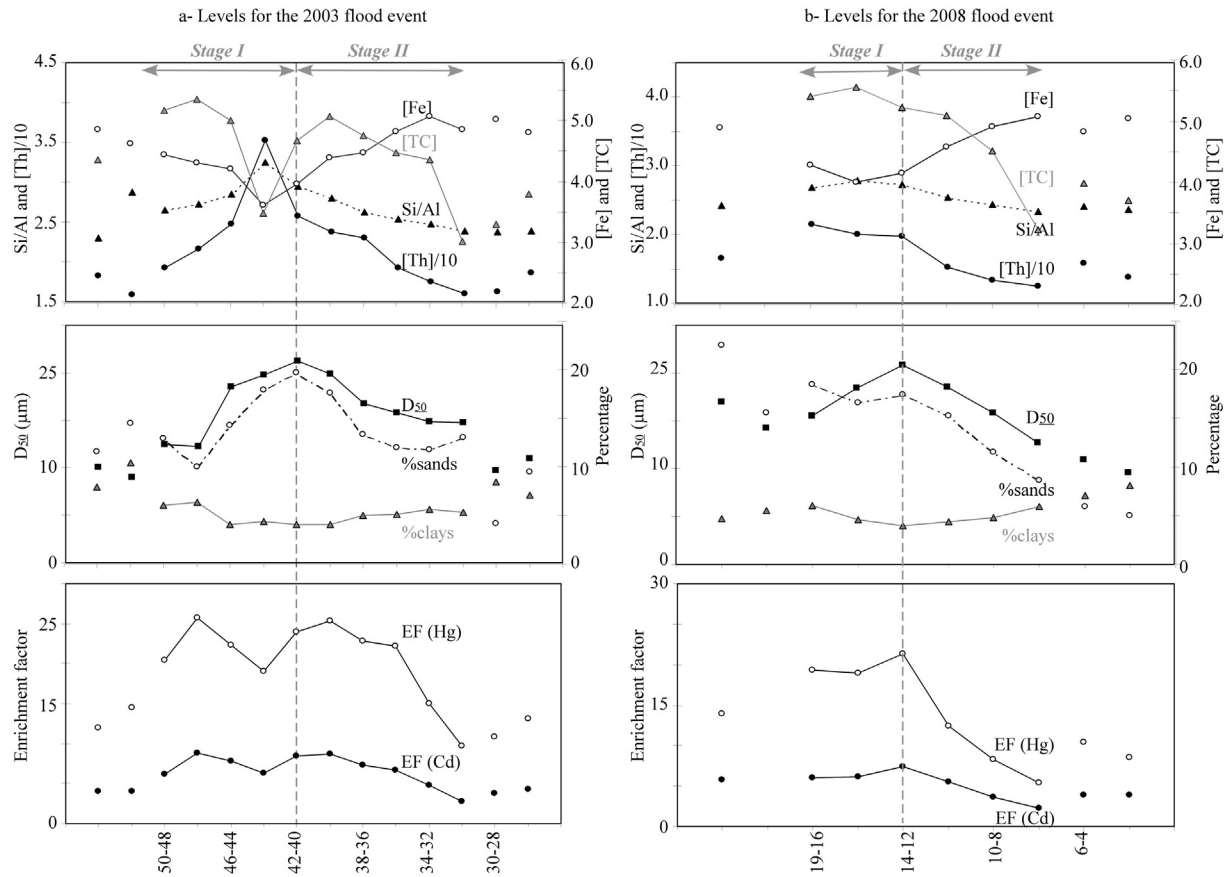

Fig. 5. Vertical profile of Cd and Hg enrichment factors (see text for calculation) in sedimentary unit 1 from the core.

Fig. 6. Variations in selected parameters (*Si/Al* ratio, TOC, Fe and Th concentrations, percentage of sands and clays, D$_{50}$, enrichment factors of Cd and Hg) in the core sediments during a — the 2003 flood and b — the 2008 flood.

For these flood sequences recorded in the Villerest sediments, anthropogenic enriched trace elements present significant correlations with the *Si/Al* and *TOC* contents. A short depletion of these enriched TEs clearly corresponds to a *Si/Al* maximum during phase I (Fig. 6a). The influence of coarser non-impacted detrital material, such as K-feldspars, quartz and accessory minerals, on the archived anthropogenic TE signal is highlighted here. The enriched TE decreased together with the *TOC* content although the *Fe* content kept increasing (Fig. 6a and b). Hence, the flood events mobilized TE-rich material mostly associated with the organic fraction rather than detrital (*Si/Al* variations) and Fe-rich material.

All of these detailed chemical variations enhance the importance of material origins during a flood event and the influence of grain-size and associated mineralogical effects on major and trace element concentrations, even in the <63 μm fraction. The significant relationships between the sand and clay percentages, D$_{50}$, *Si/Al*, *K/Rb* ratios and detrital trace elements show the presence of coarse particles, which mainly mobilized at the beginning of a flood in a dam reservoir, although finer particles settle at the end of the flood and influence chemical variations.

4. Conclusions

When study areas such as the Loire River are located in artificially narrowing rivers with sandy sediment, fine-grained sediment settling spots are difficult to find and reservoirs can be considered for well-defined sedimentary archives. In the Villerest flood-control reservoir, the sedimentological analysis of the studied core allows us to highlight different settling periods relative to the dam's construction, operation phase and upstream hydrological conditions. The base of this sedimentary archive illustrates local aggradation conditions associated with dam construction and water infilling periods. Only the upper sedimentary unit, which was deposited in a lacustrine context during dam operation, can be taken into account to describe the temporal dynamics of the pollutants. In addition, major flood events during the 1984–2010 period have largely contributed to sedimentary infill (43% of the total sediment accumulation since 1984) with highly TE-impacted deposits (EF >20 for Hg and >10 for Cd and Bi) compared to interflood periods. When considering a linear sedimentation rate over the period, such an influence from the flood events could not be indicated, and the flood sequences were wrongly associated with high polluted periods and specific anthropogenic inputs. Hence, these results emphasize the importance of combining sedimentological and geochemical analyses to understand the sedimentary infilling processes and temporal trajectories of contaminants in a reservoir.

The flood sequences resulting from sediment-laden underflows present variations in the sedimentological and geochemical signals. Grain-size variations and conservative TE inputs mark two stages associated with flood hydrograms. In particular, an increasing discharge stage is associated with a coarsening phase with important detrital material inputs, although the decreasing discharge stage presents a fining particle size trend and a depletion of detrital inputs followed by Fe-rich clay deposits. For all of the flood episodes, anthropogenic TE possibly came from remnant sources, solicited and/or emphasized. In addition, even in the <63 μm fraction of these flood sequences, the anthropogenic TE signals appear to be controlled by the grain-size and detrital material inputs. Indeed, massive inputs of coarser and non-impacted sediments at maximum discharge induce an underestimation of the calculated EF. In terms of river dam management, these results show the importance of flood control and limiting the spread of pollutants, though the dam reservoir also constitutes important stocks of polluted sediments, which can potentially be remobilized during reworking phases and/or storage variations.

Acknowledgments

References

Alvarez-Iglesias, P., Quintana, B. Rubio, Pérez-Arlucea, M., 2007. Sedimentation rates and trace metal input history in intertidal sediments from San Simón Bay (Ría de Vigo, NW Spain) derived from ^{210}Pb and ^{137}Cs chronology. J. Environ. Radioact. 98, 229–250.

Ambers, R.K.R., 2001. Using the sediment record in a western Oregon flood-control reservoir to assess the influence of storm history and logging on sediment yield. J. Hydrol. 244, 181–200.

Arnaud-Fassetta, G., 2003. River channel changes in the Rhone Delta (France) since the end of the Little Ice Age: geomorphological adjustment to hydroclimatic change and natural resource management. Catena 51, 141–172.

Audry, S., Schäfer, J., Blanc, G., Jouanneau, J.-M., 2004. Fifty-year sedimentary record of heavy metal pollution (Cd, Zn, Cu, Pb) in the Lot River reservoirs (France). Environ. Pollut. 132, 413–426.

Audry, S., Grosbois, C., Bril, H., Schäfer, J., Kierczak, J., Blanc, G., 2010. Post-depositional redistribution of trace metals in reservoir sediments of a mining/smelting-impacted watershed (the Lot River, SW France). Appl. Geochem. 25, 778–794.

Bábek, O., Hilscherová, K., Nehyba, S., Zeman, J., Famera, M., Francu, J., Holoubek, I., Machát, J., Klánová, J., 2008. Contamination history of suspended river sediments accumulated in oxbow lakes over the last 25 years. J. Soils Sediments 8, 165–176.

Bábek, O., Faměra, M., Hilscherová, K., Kalvoda, J., Dobrovolný, P., Sedláček, J., Machát, J., Holoubek, I., 2011. Geochemical traces of flood layers in the fluvial sedimentary archive; implications for contamination history analyses. Catena 87, 281–290.

Benoit, G., Rozan, T.F., 2001. ^{210}Pb and ^{137}Cs dating methods in lakes: a retrospective study. J. Paleolimnol. 25, 455–465.

Blott, S.J., Pye, K., 2001. GRADISTAT: a grain size distribution and statistics package for the analysis of unconsolidated sediments. Earth Surf. Process. Landf. 26, 1237–1248.

Bouchez, J., Gaillardet, J., France-Lanort, C., Dutra-Maia, P., Maurice, P., 2011. Grain size control of river suspended sediment geochemistry: clues from Amazon River depth-profiles. Geochem. Geophys. Geosyst. 12, Q03008. http://dx.doi.org/10.1029/2010GC003380.

Bravard, J.-P., Goichot, M., Tronchère, H., 2013. An assessment of sediment-transport processes in the Lower Mekong River based on deposit grain sizes, the CM technique and flow-energy data. Geomorphology http://dx.doi.org/10.1016/2013.

Callender, E., 2003. Heavy metals in the environment. Historical trends. In: Sherwood collar, B. (Ed.), Treatise on Geochemistry. 9, pp. 67–105.

Castelle, S., Schäfer, J., Blanc, G., Audry, S., Etcheber, H., Lissalde, J.-P., 2007. 50-year record and solid state speciation of mercury in natural and contaminated reservoir sediment. Appl. Geochem. 22, 1359–1370.

Chen, C.-T., Kandasamy, S., 2007. Evaluation of elemental enrichments in surface sediments off southwestern Taiwan. Environ. Geol. 54, 1333–1346.

Claude, N., Rodrigues, S., Bustillo, V., Bréhéret, J.-G., Macaire, J.-J., Jugé, P., 2012. Estimating bedload transport in a large sand–gravel bed river from direct sampling, dune tracking and empirical formulas. Geomorphology 179, 40–57.

Coynel, A., Schäfer, J., Blanc, G., Bossy, C., 2007. Scenario of particulate trace metal and metalloid transport during a major flood event inferred from transient geochemical signals. Appl. Geochem. 22, 821–836.

Dacharry, M., 1974. Hydrologie de la Loire en amont de Gien. 2. N.A.L., Paris (334 & 285 pp.).

Dai, S.B., Yang, S.L., Cai, M., 2008. Impacts of dams on the sediment flux of the Pearl River, southern China. Catena 76, 36–43.

Desmet, M., et al., 2012. Spatial and temporal trends in PCBs in sediment along the lower Rhône River, France. Sci. Total Environ. 433, 189–197.

Dill, H.G., 2010. The "chessboard" classification scheme of mineral deposits: mineralogy and geology from aluminum to zirconium. Earth Sci. Rev. 100, 1–420.

Fan, J., Morris, G.L., 1992. Reservoir sedimentation. I: delta and density current deposits. J. Hydraul. Eng. 118, 354–369.

Folk, R.L., Ward, W.C., 1957. Brazos River bar: a study in the significance of grain size parameters. J. Sediment. Petrol. 27, 3–26.

Gilli, A., Anselmetti, F.S., Glur, L., Wirth, S.B., 2013. Lake sediments as archives of recurrence rates and intensities of past flood events. In: Schneuwly-Bollschweiler, M., Stoffel, M., Rudolf-Miklau, F. (Eds.), Dating torrential processes on fans and cones — methods and their application for hazard and risk assessmentAdvances in Global Change Research 47. Springer, pp. 225–242.

Giovanoli, F., 1990. Horizontal transport and sedimentation by interflows and turbidity currents in Lake Geneva. In: Tilzer, M.M., Serruya, C. (Eds.), Large lakes: ecological structure and function. Springer, Berlin/Heidelberg, pp. 175–195.

Govindaraju, K., Mervelle, G., 1987. Fully automated dissolution and separation methods for inductively coupled plasma atomic emission spectrometry rock analysis. Application to the determination of rare earth elements. J. Anal. At. Spectrom. 2, 615–621.

Govindaraju, K., Potts, P., Webbs, J.S., Watson, J., 1994. Whin sill dolerite WS-E from England and Pitscurrie microgabbro PM-S from Scotland: assessment by one hundred and four international laboratories. Geostand. Newslett. 18, 221–300.

Grosbois, C., Meybeck, M., Lestel, L., Lefèvre, I., Moatar, F., 2012. Severe and contrasted polymetallic contamination patterns (1900–2009) in the Loire River sediments (France). Sci. Total Environ. 435–436, 290–305.

Grousset, F.E., Cortijo, E., Huon, S., Hervé, L., Richter, T., Burdloff, D., Duprat, J., Weber, O., 2001. Zooming in on Heinrich layers. Paleoceanography 16, 240–259.

Horowitz, A.J., Elrick, K.A., 1987. The relation of stream sediment surface area, grain size and composition to trace element chemistry. Appl. Geochem. 2, 437–451.

Kabata-Pendias, A., 2000. Trace Elements in Soils and Plants, 3rd ed. CRC Press.

Klaminder, J., Appleby, P., Crook, P., Renberg, I., 2012. Post-deposition diffusion of 137 Cs in lake sediment: implications for radiocaesium dating. Sedimentology 59, 2259–2267.

Le Cloarec, M.F., Bonte, P., Lestel, L., Lefèvre, I., Ayrault, S., 2011. Sedimentary record of metal contamination in the Seine River during the last century. Phys. Chem. Earth 36, 515–529.

Macaire, J.J., Gay-Ovejero, I., Bacchi, M., Cocirta, C., Patryl, L., Rodrigues, S., 2013. Petrography of alluvial sands as a past and present environmental indicator: case of the Loire River (France). Int. J. Sed. Res. 28, 285–303.

Morris, G.L., Annandale, G., Hotchkiss, R., 2008. Reservoir Sedimentation. Sedimentation Engineering Process Measurements, Modeling and Practices. Amer Soc Civil Engineer (ASCE), Reston, USA, pp. 1–17.

Mourier, B., Desmet, M., Van Metre, P.C., Mahler, B.J., Perrodin, Y., Roux, G., Bedell, J.-P., Lefèvre, I., Babut, M., 2014. Historical records, sources and spatial trends of PCBs along the Rhône River (France). Sci. Total Environ. 476–477, 568–576.

Pacyna, J.M., Pacyna, E.G., 2001. An assessment of global and regional emissions of trace metals to the atmosphere from anthropogenic sources worldwide. Environ. Rev. 9, 269–298.

Passega, R., 1957. Texture as characteristic of clastic deposition. Bull. Am. Assoc. Pet. Geol. 41, 1952–1984.

Passega, R., 1964. Grain-size representation by CM pattern as a geological tool. J. Sediment. Petrol. 34, 830–847.

Pye, K., Blott, S.J., 2004. Particle size analysis of sediments, soils and related particulate materials for forensic purposes using laser granulometry. Forensic Sci. Int. 144, 19–27.

Smith, J.T., Clarke, R.T., Saxén, R., 2000. Time-dependent behavior of radiocaesium: a new method to compare the mobility of weapons test and Chernobyl derived fallout. J. Environ. Radioact. 79, 65–83.

Sturm, M., Matter, A., 1978. Turbidites and varves in Lake Brienz (Switzerland): deposition of clastic detritus by density currents. Int. Assoc. Sedimentol. Spec. Publ. 2, 147–168.

Valverde, L., Jugé, P., Handfus, T., 2013. Résultats granulométriques et localisation des points durs en Loire. rapport InfoSed 2, p. 180.

Van Metre, P.C., Wilson, J.T., Fuller, C.C., Callender, E., Mahler, B.J., 2004. Collection, analysis, and age-dating of sediment cores from 56 U.S. lakes and reservoirs sampled by the U.S. geological survey, 1992–2001. USGS Scientific Investigations Report–5184.

Vörösmarty, C.J., Michel Meybeck, B., Fekete, K., Sharma, P. Green, Syvitski, J.P., 2003. Anthropogenic sediment retention: major global impact from registered river impoundments. Glob. Planet. Chang. 39, 169–1907.

Vukovic, D., Vukovic, Z., Stankovic, S., 2014. The impact of the Danube Iron Gate Dam on heavy metal storage and sediment flux within the reservoir. Catena 113, 18–23.

Walling, D.E., Bradley, S.B., 1990. Some applications of caesium-137 measurements in the study of fluvial erosion, transport and deposition. In: Walling, D.E., Yair, A., Berkowicz, S. (Eds.), Erosion, Transport and Deposition Processes, (Proc. Jerusalem Workshop, April 1987), IAHS Publ. 189. IAHS Press, Wallingford, UK, pp. 179–203.

Walling, D.E., He, Q., 1997. Sediment deposition on river floodplains. 29, pp. 263–282.

Walling, D.E., He, Q., 1998. The spatial variability of overbank sedimentation on river floodplains. Geomorphology 24, 209–223.

Walling, D.E., Owens, P.N., Leeks, G.J.L., 1997. The characteristics of overbank deposits associated with a major flood event in the catchment of the River Ouse, Yorkshire, UK. Catena 31, 53–75.

Walling, D.E., Owens, P.N., Carter, J., Leeks, G.J.L., Lewis, S., Meharg, A.A., Wright, J., 2003. Storage of sediment-associated nutrients and contaminants in river channel and floodplain systems. Appl. Geochem. 18, 195–220.

Yang, S., Zhao, Q., Belkin, I.M., 2002. Temporal variation in the sediment load of the Yangtze River and the influences of human activities. J. Hydrol. 263, 56–71.

Ye, C., Li, S., Zhang, Y., Zhang, Q., 2011. Assessing soil heavy metal pollution in the water-level-fluctuation zone of the Three Gorges Reservoir, China. J. Hazard. Mater. 191, 366–372.

Ziegler, C.K., Nisbet, B.S., 1995. Long-term simulation of fine-grained sediment transport in large reservoir. J. Hydraul. Eng. 121, 773–781.